

How Flow Changes Polymer Depletion in a Slit

Takashi Taniguchi¹, Yuichiro Arai¹, Remco Tuinier^{2,3}, and Tai-Hsi Fan⁴

¹ Graduate School of Engineering, Kyoto University Katsura Campus, Nishikyo-ku, Kyoto 615-8510, JAPAN

² DSM ChemTech, ACES, P.O. Box 18, 6160 MD Geleen, The Netherlands

³ Van 't Hoff Laboratory for Physical and Colloid Chemistry, Debye Institute, Utrecht University, The Netherlands

⁴ Department of Mechanical Engineering, University of Connecticut, CT 06269, USA

Received: date / Revised version: date

Abstract. A theoretical model is developed for predicting dynamic polymer depletion effects under the influence of fluid flow. The results are established by combining the two-fluid model and the self-consistent field theory. We consider a uniform fluid flow across a slit containing a solution with polymer chains. The two parallel and infinitely long walls are permeable to solvent only and the polymers do not adsorb to these walls. For a weak flow and a narrow slit in Θ -solvent conditions, an analytic expression is derived to describe the steady state polymer concentration profiles. In both Θ - and good-solvents, we compute the time evolution of the concentration profiles for various flow rates characterized by the Peclet number. The model reveals the interplay of depletion, solvent condition, slit width, and relative strength of the fluid flow.

1 Introduction

In a polymer solution near an interface the polymer segments are either attracted or repelled by that interface [1]. In the latter case there exists a depletion zone near the interface. In this zone the polymer segment concentration is smaller than the bulk value because the possible number of configurations of the polymer chains is reduced. The non-adsorbing wall forbids a certain amount of paths of the polymer chain. For ideal polymer chains near a hard wall the depletion thickness is close to the polymer's radius of gyration [2]. This result holds generally for a dilute polymer solution [3,4], whereas in a semi-dilute polymer solution the depletion thickness is determined by the correlation length [5]. These results for the dilute and semi-dilute concentration regimes were later combined [6, 7]. The investigations of polymer depletion at an interface were primarily focused on the equilibrium case in the past. The equilibrium depletion thickness suffices to describe the attraction between colloidal particles when the depletion layers overlap [8,9], which can be measured for instance by optical tweezers [10]. The depletion force may yield phase transitions [11–13] for which the binodals can be predicted for well-defined colloid-polymer mixtures [14, 4]. It is of fundamental and practical interest to understand the change of the depletion layer under a fluid flow effect (Fig.1). Simple shear flow of a polymer solution next to a single wall leads to slip even if the depletion layer is assumed to be unaffected by shear [15]. It has been shown, however, that the flow does affect the depletion thickness

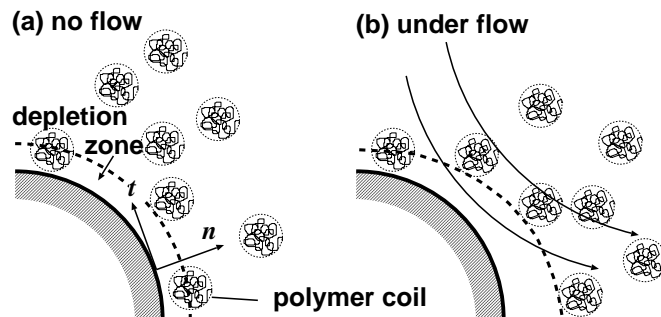


Fig. 1. Convective depletion effect for polymer chains near a non-adsorbing solid surface (a) under no flow and (b) under flow. n and t denote unit normal and tangential vectors to the surface.

at a wall [24]. At the particle level, the models developed for the single particle motion and pairwise particle interactions [25–27] neglect the slight distortion of the depletion zone, which is applicable for long-time Brownian diffusion with weak convective effect. A convective depletion model was first established by Odijk [28] for describing a thin depletion boundary layer in front of a fast moving sphere. A complete picture of the fully coupled convective depletion effect under various solution conditions is not yet available.

The flow of a polymer solution near an interface is an important practical phenomenon [16,17]. To give a few examples, in oil recovery, aqueous polymer solutions are used to sweep oil out of natural porous media in the earth's subsurface [18]. In that situation the polymer solution flows

through narrow pores where a large effective viscosity, as enhanced by the presence of the polymers, is required to flush oil out. Measurements of apparent polymer solution viscosity obtained from flow through narrow pores indicate that the viscosity is reduced compared to the bulk viscosity, see e.g. Chauveteau [19] and Omari et al. [20]. Capillary rheometry is another example [21]. It uses the fact that the flow time is proportional to the liquid viscosity. However, for polymer solutions the relative viscosity from capillary rheometry may differ from other methods [21–23]. These are all related to dynamic depletion effects in confined geometries.

In this paper we propose a theoretical framework to investigate dynamic depletion effects. We study the influence of flow on the polymer segment density profile in a narrow or wide slit. This is an interesting problem since for a narrow slit an analytical expression is available only for the equilibrium segment density profile [29, 1, 6]. It is unclear yet to what extent a flow field modifies the depletion layers. To resolve the interplay of convective and diffusive effects, we start from a general formulation of the two-fluid model proposed by Doi and Onuki [30] for polymer transport. Then we apply the ground state approximation (GSA) to the self-consistent field theory (SCFT) and the dynamics version of SCFT to express the chemical potential of polymer segments under various flow conditions. This framework allows us to clarify how the segment density is altered upon increasing flow. It will tell for which Peclet numbers fluid flow significantly affects polymer depletion as compared to the equilibrium case. A detailed analysis for Θ - and good-solvent cases is provided in the results and discussion section.

2 Theory

2.1 Two-Fluid Model

We consider inertialess fluid motion and free draining polymers in dilute to semi-dilute polymer solutions. The transient evolution of polymer segment volume fraction ϕ_p is given by the equation of continuity:

$$\frac{\partial \phi_p(\mathbf{r}, t)}{\partial t} = -\nabla \cdot (\phi_p \mathbf{v}_p), \quad (1)$$

where t is time, \mathbf{v}_p is the velocity of the polymer segments in the fluid, $\phi_p(\mathbf{r}, t) = a^3 \rho_p(\mathbf{r}, t)$ with a being the segment length and ρ_p the local number density of polymer segment. The local volume fraction of solvent is ϕ_s . Because $\phi_p + \phi_s = 1$, the total velocity $\mathbf{v}(\mathbf{r}, t) = \phi_p \mathbf{v}_p + \phi_s \mathbf{v}_s$ (\mathbf{v}_s is the solvent velocity) satisfies the incompressibility condition $\nabla \cdot \mathbf{v} = 0$. The momentum equation of the two-fluid model can be derived from the Rayleighian given by Doi and Onuki [30]:

$$\mathcal{R} = \int \left[\frac{\zeta(\mathbf{r}, t)}{2} |\mathbf{v}_p - \mathbf{v}_s|^2 - \mu_p \nabla \cdot (\phi_p \mathbf{v}_p) - \mu_s \nabla \cdot (\phi_s \mathbf{v}_s) - p \nabla \cdot \mathbf{v} + \boldsymbol{\sigma}_p : \nabla \mathbf{v}_p + \boldsymbol{\sigma}_s : \nabla \mathbf{v}_s \right] d\mathbf{r}, \quad (2)$$

where $\mu_p, \mu_s, \boldsymbol{\sigma}_p, \boldsymbol{\sigma}_s$, and p are the local chemical potential of polymer and solvent, the deviatoric stress of polymer and solvent, and the hydrodynamic pressure, respectively. The friction coefficient ζ between the two fluids can be defined as $\zeta = 6\pi\eta_s \xi / \xi^3$, where $\xi(\phi_p)$ is the blob size and η_s is the solvent viscosity. The blob size is related to ϕ_p as $\xi \simeq a\phi_p^{-m}$ [5], where $m = 1$ and $3/4$ for Θ - and good solvent, respectively. By minimizing \mathcal{R} with respect to \mathbf{v}_p and \mathbf{v}_s , the following momentum equations can be derived [30]:

$$\zeta(\mathbf{v}_p - \mathbf{v}_s) + \phi_p \nabla p + \phi_p \nabla \mu_p - \nabla \cdot \boldsymbol{\sigma}_p = 0, \quad (3)$$

$$\zeta(\mathbf{v}_s - \mathbf{v}_p) + \phi_s \nabla p + \phi_s \nabla \mu_s - \nabla \cdot \boldsymbol{\sigma}_s = 0. \quad (4)$$

By combining Eqs.(3) and (4) we obtain

$$\nabla \cdot \boldsymbol{\sigma} - \nabla P - \nabla \cdot \boldsymbol{\pi} = 0, \quad (5)$$

where the total stress $\boldsymbol{\sigma} = \boldsymbol{\sigma}_p + \boldsymbol{\sigma}_s$, P is the modified pressure defined by $P = p + \mu_s$, and $\boldsymbol{\pi}$ is the osmotic pressure tensor defined as

$$\nabla \cdot \boldsymbol{\pi} = \phi_p(\mathbf{r}, t) \nabla \mu(\mathbf{r}, t), \quad (6)$$

where $\mu = \mu_p - \mu_s$ is the difference between the chemical potentials. Substituting Eq.(5) into Eq.(4) and eliminating P , the following expression for the polymer velocity is obtained:

$$\mathbf{v}_p \simeq \mathbf{v} - \frac{\phi_s}{\zeta} \left[\phi_s (\nabla \cdot \boldsymbol{\pi} - \nabla \cdot \boldsymbol{\sigma}_p) + \phi_p \nabla \cdot \boldsymbol{\sigma}_s \right]. \quad (7)$$

In this paper we consider $\phi_p \ll 1$ for dilute and semi-dilute solutions, and $\phi_p \nabla \cdot \boldsymbol{\sigma}_s$ of the above equation is negligible. The polymer velocity relative to the total velocity is driven by the osmotic pressure and the deviatoric stress of the polymer fluid. Substituting Eq.(7) into Eq.(1) yields the polymer transport equation [30]:

$$\frac{\partial \phi_p}{\partial t} + \nabla \cdot (\phi_p \mathbf{v}) \simeq \nabla \cdot \left[\frac{\phi_p \phi_s^2}{\zeta(\phi_p)} \left(\phi_p \nabla \mu - \nabla \cdot \boldsymbol{\sigma}_p \right) \right]. \quad (8)$$

This formulation is consistent with Odijk's work [28] except for the ϕ_p -dependent friction coefficient and the additional $\nabla \cdot \boldsymbol{\sigma}_p$ term. For a solid object with an arbitrary shape, the osmosis-induced force and torque are $\mathbf{f} = \int_{\partial\Omega} (-\boldsymbol{\pi} \cdot \mathbf{n}) dS$ and $\mathbf{T} = \int_{\partial\Omega} \mathbf{R} \times (-\boldsymbol{\pi} \cdot \mathbf{n}) dS$, respectively, where \mathbf{R} is a vector to the surface of the object from the center of gravity of it.

Assuming that the polymer stress in the dilute and semi-dilute ($\bar{\phi}_p \lesssim$ overlap fraction $\phi_p^* \simeq N^{1-3\nu}$) polymer solution can be expressed as $\eta' \phi_p (\nabla \mathbf{v} + (\nabla \mathbf{v})^T)$ where η' is a constant, the total velocity follows as $\mathbf{v} \sim \mathcal{O}(\bar{\phi}_p^2)$, as seen from Eq.(5) and $\boldsymbol{\pi} \sim \mathcal{O}(\bar{\phi}_p^2)$, and thus $\nabla \cdot \boldsymbol{\sigma}_p \sim \mathcal{O}(\bar{\phi}_p^3)$. Also because $\mu \sim \mathcal{O}(\bar{\phi}_p)$, so $\phi_p \nabla \mu \sim \mathcal{O}(\bar{\phi}_p^2)$, this implies $\mathcal{O}(\nabla \cdot \boldsymbol{\sigma}_p) \ll \mathcal{O}(\phi_p \nabla \mu)$ and the polymer force $\nabla \cdot \boldsymbol{\sigma}_p$ in Eq.(8) is indeed negligible [28].

2.2 Chemical Potential of Polymers

From the self-consistent field theory (SCFT) and the ground state approximation (GSA), the Helmholtz free energy of the mixture can be expressed as [5]

$$F = \epsilon_o \int \left[\frac{C}{2} (\nabla \sqrt{\phi_p})^2 + f_o(\phi_p) \right] d\mathbf{r}, \quad (9)$$

where $\epsilon_o = k_B T / a^3$, $C = a^2 / 3$, $f_o(\phi_p) = (1 - \phi_p) \ln(1 - \phi_p) + \chi \phi_p (1 - \phi_p)$, and χ is the Flory-Huggins parameter. In a good solvent $\chi = 0$, whereas $\chi = 1/2$ corresponds to Θ -solvent conditions. The chemical potential difference μ is determined by the functional derivative of F with respect to ϕ_p [28] :

$$\mu(\mathbf{r}) = \epsilon_o \left[-\frac{C}{2\sqrt{\phi_p}} \nabla^2 \sqrt{\phi_p} + (1 - 2\chi)\phi_p \right]. \quad (10)$$

Since ϕ_p is much smaller than unity, only the zeroth- and first-order terms involving ϕ_p in the chemical potential are preserved. The corresponding osmotic stress tensor π_{ij} , which is scaled by ϵ_o , can be expressed as

$$\pi_{ij} = \left\{ \left[\pi_o - \frac{C}{2} \nabla \cdot (\sqrt{\phi_p} \nabla \sqrt{\phi_p}) \right] \delta_{ij} + C \frac{\partial \sqrt{\phi_p}}{\partial x_i} \frac{\partial \sqrt{\phi_p}}{\partial x_j} \right\}, \quad (11)$$

where $\pi_o(\phi_p) = \phi f'_o(\phi_p) - f_o$ is the osmotic pressure in the bulk. Note that $\nabla \cdot \boldsymbol{\pi}$ satisfies Eq.(6).

Without GSA, the Helmholtz free energy is expressed as

$$\frac{F}{k_B T} = \frac{1}{a^3} \int \left[\chi \phi_p \phi_s - w_p \phi_p - w_s \phi_s \right] d\mathbf{r} - \frac{\bar{\phi}_p}{N} \ln \left(\frac{N Q_p}{V \phi_p} \right) - \frac{\bar{\phi}_s}{N} \ln \left(\frac{Q_s}{V \phi_s} \right), \quad (12)$$

where N is the number of segment in a single chain, V is the volume of the system, and w_α and $\bar{\phi}_\alpha$ are the dimensionless local interaction field (scaled by $k_B T$) and the average volume fraction of polymer segments in the bulk for the α -component (α represents polymer or solvent), respectively. The partition functions Q_p and Q_s for a single chain and a single solvent, respectively, are defined by

$$Q_p = \int_V d\mathbf{r} \int_0^1 q(\mathbf{r}, s) q(\mathbf{r}, 1-s) ds, \quad (13)$$

and

$$Q_s = \int_V d\mathbf{r} \exp(-w_s(\mathbf{r})). \quad (14)$$

In Eq.(13), q is the statistical weight of the polymer chain and can be calculated by

$$\frac{\partial q}{\partial s} = \frac{a^2}{6} N \nabla^2 q - N w_p(\mathbf{r}) q \quad \text{for } 0 \leq s \leq 1 \quad (15)$$

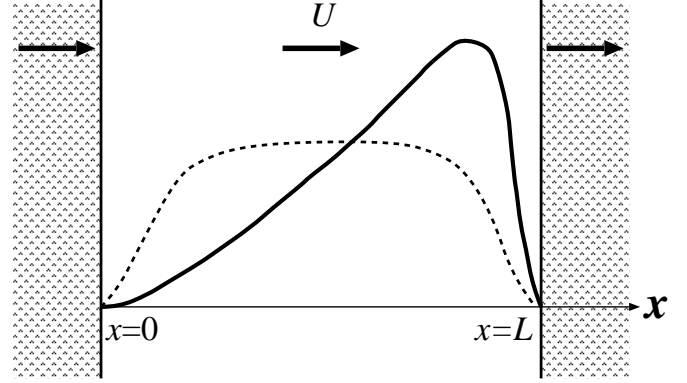


Fig. 2. A schematic illustration of the convective depletion effect on the polymer segment profile (solid line) in a slit between two parallel and solvent permeable walls. The dashed line indicates the equilibrium distribution. The polymer concentration vanishes at the walls.

with the initial condition $q(\mathbf{r}, 0) = 1$ and the zero boundary condition at the solid surface $q(\mathbf{r} \in \partial\Omega) = 0$ for an arbitrary contour coordinate s .

In order to evaluate μ_p and μ_s for a given $\phi_p(\mathbf{r}, t)$, the following iterative procedure can be used [31]:

i) Find $w_p(\mathbf{r})$ and $q(\mathbf{r}, s)$ that satisfy Eq.(15) and

$$\frac{1}{Q_p} \int_0^1 q(\mathbf{r}, s) q(\mathbf{r}, 1-s) ds = \frac{1}{V \phi_p} \phi_p(\mathbf{r}, t) \quad (16)$$

along with the initial and boundary conditions.

ii) Evaluate $w_s(\mathbf{r})$ that satisfies

$$\frac{1}{Q_s} \exp(-w_s(\mathbf{r})) = \frac{1}{V \phi_s} \phi_s(\mathbf{r}, t). \quad (17)$$

iii) Compute the chemical potential difference $\mu = \mu_p - \mu_s$ from the functional derivatives:

$$\mu_p(\mathbf{r}) = \frac{\delta F}{\delta \phi_p} = -w_p(\mathbf{r}) + \chi \phi_s(\mathbf{r}), \quad (18)$$

$$\mu_s(\mathbf{r}) = \frac{\delta F}{\delta \phi_s} = -w_s(\mathbf{r}) + \chi \phi_p(\mathbf{r}). \quad (19)$$

iv) Finally, the time evolution of $\phi_p(\mathbf{r}, t)$ can be calculated by Eq.(8) with $\boldsymbol{\sigma}_p = \mathbf{0}$.

3 Results and Discussion

We focus on non-equilibrium concentration profiles under a uniform flow passing through two parallel and solvent-permeable walls (Fig.2). Both transient and steady state results are provided next. In this one-dimensional problem, the length is scaled by $\ell = (a^2/6)^{1/2}$ and the time scale is defined by $\tau = \ell^2/D$, where the diffusion constant $D = k_B T / 6\pi\eta_s a$. The volume fraction of polymer is scaled

by the averaged volume fraction $\bar{\phi}_p$, and the chemical potential is scaled by $k_B T/a^3$. Hereafter we use dimensionless expressions. The scaled chemical potential difference is expressed as

$$\mu = -\frac{1}{\bar{\phi}} \nabla^2 \varphi + v \varphi^2, \quad (20)$$

where $v = (1 - 2\chi)\bar{\phi}_p$ and $\varphi = (\phi_p)^{1/2}$. Note that the ground-state approximation, Eq.(20), for Θ -solvent is valid only for a narrow slit $L/R_g < \pi$ [5], where $R_g = a(N/6)^{1/2}$. The polymer transport equation (Eq.(8)) thus can be expressed as

$$\frac{\partial \varphi^2}{\partial t} + \text{Pe} \frac{\partial \varphi^2}{\partial x} = \bar{\phi}_p^{(1-2m)} \frac{\partial}{\partial x} \left[\varphi^{2(2-2m)} \frac{\partial \mu}{\partial x} \right], \quad (21)$$

where $\text{Pe} = U\ell/D$ is the Peclet number, and U is the uniform velocity. The corresponding boundary conditions are $\varphi(0) = 0$ and $\varphi(L) = 0$. Because the walls are not permeable for polymers, the zero flux boundary conditions $d\mu/dx|_{x=0} = 0$ and $d\mu/dx|_{x=L} = 0$ are applied. Equation (21) leads to the steady state solution:

$$\mu(x) - \mu(0) = \text{Pe} \bar{\phi}_p^{2m-1} \int_0^x \varphi^{2(2m-1)}(x') dx'. \quad (22)$$

Under a weak flow condition, $\text{Pe} \ll 1$, the first-order approximation of the steady state solution for φ and μ can be written as

$$\varphi(x) = \sqrt{\phi_p(x)} \simeq \varphi_o(x) + \text{Pe} \varphi_1(x), \quad (23)$$

and

$$\mu(x) \simeq \mu_o(x) + \text{Pe} \mu_1(x). \quad (24)$$

By substituting Eqs.(23) and (24) into Eq.(22), the corresponding leading and first-order equations become

$$\frac{d^2 \varphi_o}{dx^2} - v \varphi_o^3 + \mu_o(0) \varphi_o = 0, \quad (25)$$

and

$$\left[\frac{d^2}{dx^2} + \mu_o(0) - 3v\varphi_o^2 \right] \varphi_1 = +\varphi_o(x) \left[\mu_1(0) + \bar{\phi}_p^{2m-1} \int_0^x \varphi_o^{2(2m-1)}(x') dx' \right], \quad (26)$$

respectively. Both φ_0 and φ_1 vanish at the walls. Next we consider Θ - and good solvent cases under narrow and wide slit conditions.

3.1 Θ -solvent cases

3.1.1 Narrow slit, $L < \pi R_g$

When the distance between two walls L is smaller than πR_g , i.e., $L < \pi R_g$, the ground state approximation is

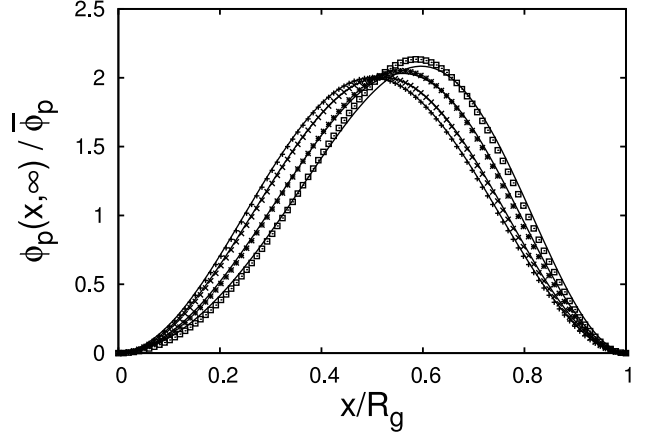


Fig. 3. Steady state polymer segment volume fraction $\phi_p(x, t = \infty)$ of a polymer solution ($\bar{\phi}_p = 0.1$, $N = 1000$ and $\chi = 0.5$) in a slit ($L/R_g = 1$, where $R_g \simeq 33\ell$) at $\text{Pe} = 0, 0.001, 0.003$, and 0.005 . The solid lines are from the numerical solutions of Eqs.(20) and (21). The symbols (+, x, *, \square) indicate the analytical approximations, respectively.

valid and we can use Eq.(20) with $v = 0$ and Eq.(21) to investigate the time evolution of polymer segment concentration profile. Under steady and weak flow conditions in Θ -solvent ($m = 1$, $\nu = 0$), Eqs.(25) and (26) reduce to

$$\frac{d^2 \varphi_o}{dx^2} = -\mu_o(0) \varphi_o, \quad (27)$$

and

$$\left[\frac{d^2}{dx^2} + \mu_o(0) \right] \varphi_1 = -\mu_1(0) \varphi_o(x) - \bar{\phi}_p \varphi_o(x) \int_0^x \varphi_o^2(x') dx'. \quad (28)$$

The zeroth-order solution corresponding to the equilibrium state [5] is

$$\varphi_o(x) = \sqrt{\phi_o(x)} = \sqrt{2} \sin\left(\frac{\pi x}{L}\right), \quad (29)$$

with $\mu_o(0) = \pi^2/L^2$, which satisfies the normalization condition, $\int_0^L \phi_o(x) dx = L$. The first order solution reads

$$\begin{aligned} \varphi_1(x) = & A \sin\left(\frac{\pi x}{L}\right) \\ & - B \left\{ \left[1 + 8\pi^2 \left(\frac{x}{L}\right) - 8\pi^2 \left(\frac{x}{L}\right)^2 \right] \cos\left(\frac{\pi x}{L}\right) \right. \\ & \left. - \cos\left(3\frac{\pi x}{L}\right) + 4\left(\frac{\pi x}{L}\right) \sin\left(\frac{\pi x}{L}\right) \right\}, \quad (30) \end{aligned}$$

where constant $B = (L/\pi)^3 \bar{\phi}_p / (16\sqrt{2})$ and $\mu_1(0)$ in Eq.(28) is found to be $-\bar{\phi}_p L/2$ by the boundary condition $\varphi_1(L) = 0$. The constant A can be determined by the normalization

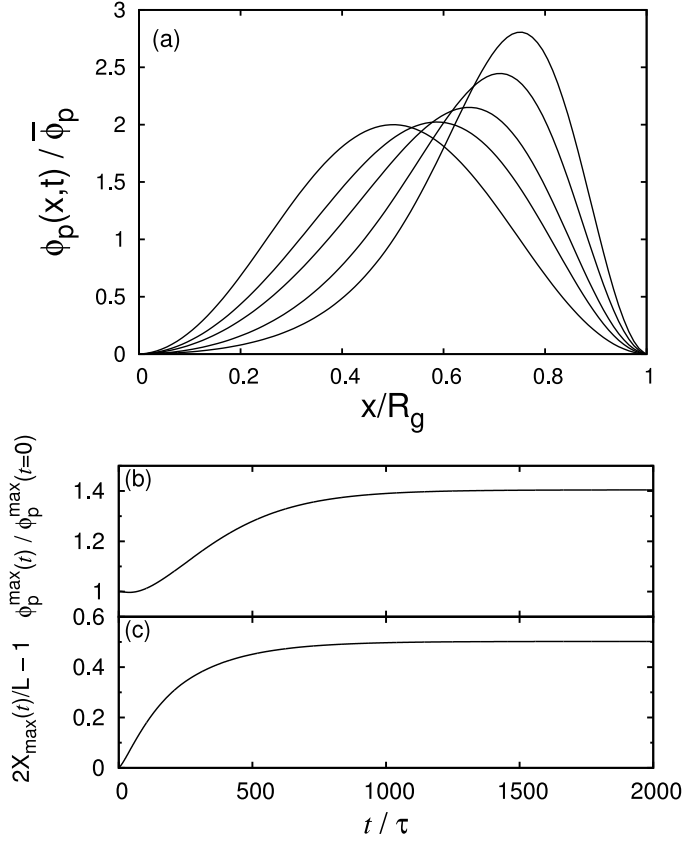


Fig. 4. (a) Transient evolutions of the segment concentration profiles $\phi_p(x,t)$, (b) the peak concentration, and (c) the peak position. Applied parameters are: $\bar{\phi}_p = 0.1$, $N = 1000$, $\chi = 0.5$, $L/R_g = 1$, and $Pe = 0.02$ at $\tilde{t} = t/\tau \geq 0^+$. The profiles shown in (a) are at $\tilde{t} = 0$ (no flow), 100, 200, 400 and 1600. At $\tilde{t} \geq 1200$, the profile approaches a steady state as can be observed in panels (b) and (c).

condition $\int_0^L \phi(x) dx = L$, and we obtain

$$A = 2\pi B + \frac{B^2}{\sqrt{2}} \left(77 - 2\pi^2 - \frac{16}{15}\pi^4 \right) Pe + \mathcal{O}(Pe^2). \quad (31)$$

Accordingly, the peak value and its location can be expressed as

$$\frac{\phi_p^{max}(Pe)}{\phi_p^{max}(0)} = 1 + B^2 \left(77 - 2\pi^2 + \frac{14}{15}\pi^4 \right) Pe^2 + \dots \quad (32)$$

and

$$x_{max} = \frac{L}{2} \left[1 + 2\sqrt{2}\pi B Pe + \mathcal{O}(Pe^3) \right]. \quad (33)$$

To demonstrate how well the first-order approximation describes the change of the concentration profile under a uniform flow, we consider the steady state case with $L/R_g = 1$ under various values of the Peclet number and compare the approximated profiles with numerical results. In Fig.3, we plot the steady state concentration profiles of

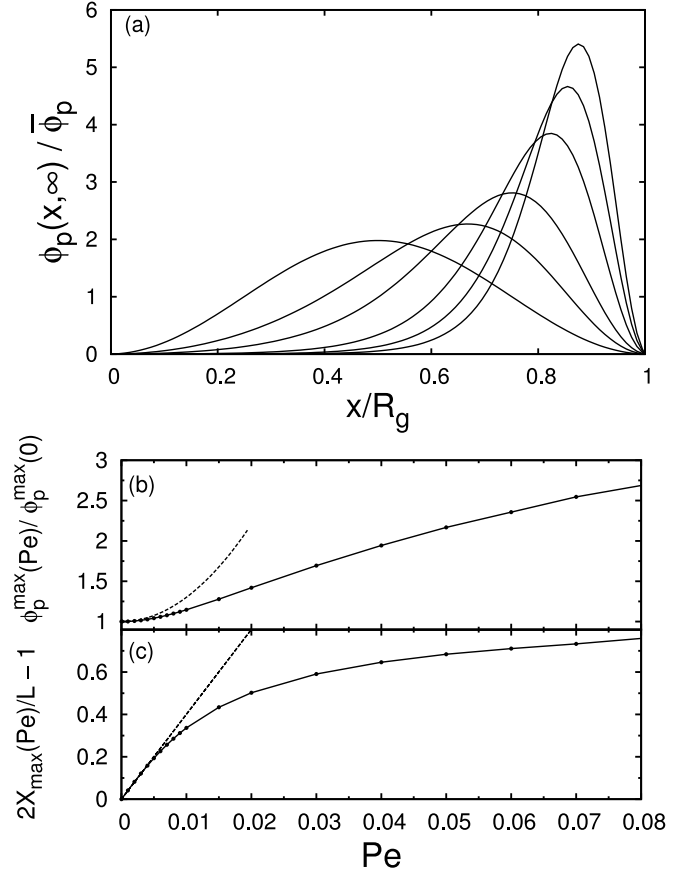


Fig. 5. (a) Steady state volume fraction profiles of polymer segments $\phi_p(x,\infty)$ in the polymer solution ($\bar{\phi}_p = 0.1$, $N = 1000$, $\chi = 0.5$ and $L/R_g = 1$) at $Pe = 0.0, 0.01, 0.02, 0.04, 0.06$, and 0.08 . (b, c) Peak polymer segment concentration $\phi_p^{max}(Pe)$ and peak position $x_{max}(Pe)$ for various Pe values. The filled circles denote the data obtained by numerical calculation using Eqs.(20) and (21) and the dotted lines follow from the perturbation method results of Eqs.(32) and (33).

polymer segment under small Peclet number flows, *i.e.*, $Pe \leq 0.005$ in a polymer solution of $N = 1000$, $\bar{\phi}_p = 0.1$ and $\chi = 0.5$. Note that $\bar{\phi}_p = 0.1$ is slightly below the overlap volume fraction $\phi_p^* \simeq 0.11$ for polymer chains with $N = 1000$. The analytical results are in good agreement with the numerical calculation for $Pe \lesssim 0.003$, but start to deviate at $Pe = 0.005$. Under weak flow conditions the first-order solution thus gives accurate results only for $Pe \lesssim 0.003$.

Figure 4 shows the transient behavior of $\phi_p(x,t)$ in a slit with $L/R_g = 1$ after imposing a fluid flow with $Pe = 0.02$ to an equilibrium profile at $t = 0$. The time evolutions of the peak value $\phi_p^{max}(t)$ and its position $x_{max}(t)$ are shown in Fig.4(b) and (c), respectively. The shift of the peak position to the steady state position is faster than that of the peak concentration, *i.e.*, firstly the peak position almost reaches to the steady state position, and then the profile of polymer segment concentration becomes sharper. This indicates that a strong convective effect applies to the polymer segments and relatively slow

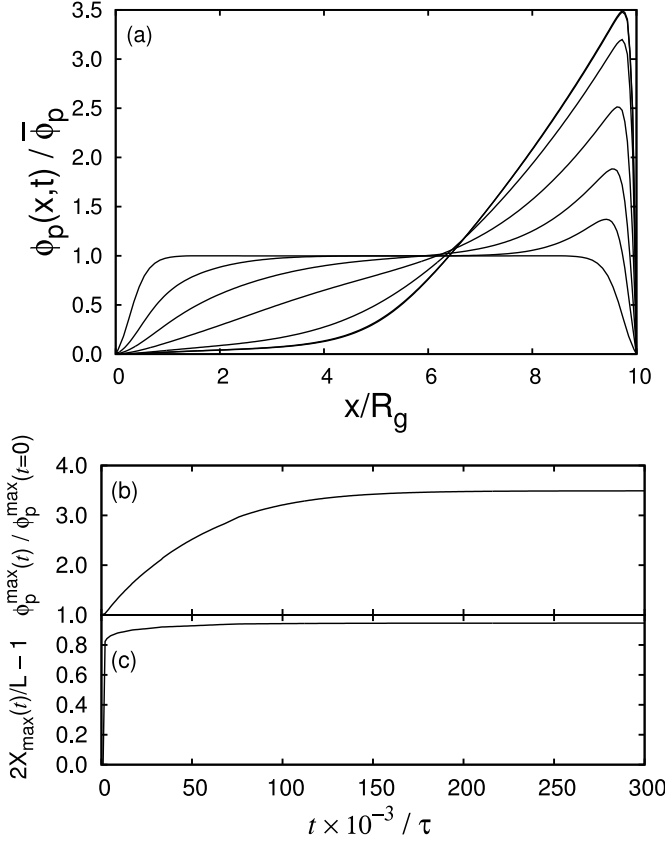


Fig. 6. (a) Transient evolutions of the segment concentration profiles $\phi_p(x, t)$, (b) the peak concentration, and (c) the peak position. Applied parameters are: $\bar{\phi}_p = 0.1$, $N = 1000$, $\chi = 0.5$, $L/R_g = 10$, and $Pe = 0.002$ at $\tilde{t} = t/\tau \geq 0^+$. The profiles are at $\tilde{t} = 0$ (no flow), 10, 25, 50, 100, 200, and 300×10^3 . At $\tilde{t} = 200 \times 10^3$, the profile reaches steady state as seen from (b) and (c), and the profiles of $\tilde{t} = 200 \times 10^3$ and $\tilde{t} = 300 \times 10^3$, are completely overlapped. Note that the results shown in Fig.4 are based on GSA, here the profiles are calculated by using the dynamic SCFT scheme.

relaxation of the polymer distribution across the slit. Next we show the steady state concentration profiles $\phi_p(x, \infty)$ evolve upon increasing the flow rate characterized by the range of $Pe = 0, 0.01, 0.02, 0.04, 0.06$, and 0.08 in a polymer solution with $\bar{\phi}_p = 0.1$, $N = 1000$ and $\chi = 0.5$ in Fig.5(a). Figure 5(b) and (c) show the peak height $\phi_p^{\max}(Pe)$ and the peak position $x_{\max}(Pe)$ of the concentration profile at steady state under various flow strength. The peak height ϕ_p^{\max} increases quadratically with Pe for small Pe as expected in Eq.(32). Above $Pe \simeq 0.05$, ϕ_p^{\max} increases linearly with Pe . In contrast to the peak height ϕ_p^{\max} , the shift of the peak position for $Pe \lesssim 0.005$ is well described by Eq.(33) as seen from Fig.5(b). For $Pe \geq 0.01$, the shift of peak position to the downstream side is suppressed. This is due to the solvent permeable wall and the accumulation of polymer chains at the downstream side.

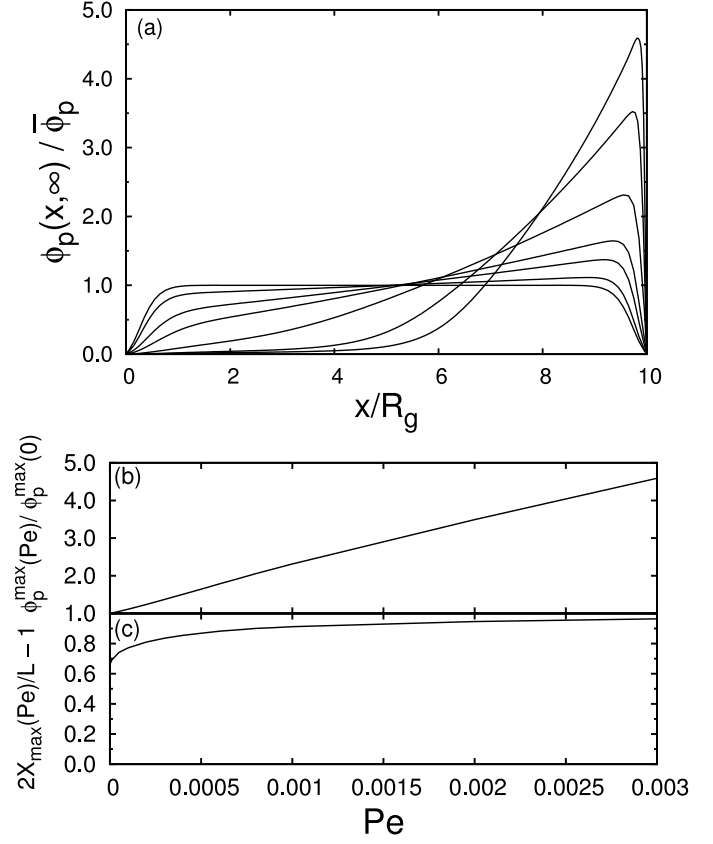


Fig. 7. (a) Steady state volume fraction profiles of polymer segments in the polymer solution ($\bar{\phi}_p = 0.1$, $N = 1000$, $\chi = 0.5$ and $L/R_g = 10$) at $Pe = 0, 1, 3, 5, 10, 20$, and 30×10^{-4} . (b, c) Change of the peak concentration $\phi_p^{\max}(Pe)$ and the peak position $x_{\max}(Pe)$ for various Pe . The data are obtained by using the dynamic SCFT scheme.

3.1.2 Wide slit, $L > \pi R_g$

When the distance L is larger than πR_g , we can not rely on GSA to evaluate the chemical potential difference $\mu(\mathbf{r})$. Here we utilize the scheme (i)-(iv) based on the self-consistent field theory explained in Sec.2.2. To demonstrate the scheme, we consider the case of $L/R_g = 10$. Firstly, we show the time evolution of the concentration profiles under $Pe = 0.002$ in Fig.6, in which the volume fraction profile of the polymer solution ($\chi = 0.5$) at a quiescent state ($Pe = 0$) coincides with the analytical result of the depletion profile near a single wall [32–34], and the peak appears near the end of the depletion zone along the downstream side. In comparison with the narrow slit case, the shift of the peak $x_{\max}(t)$ to the steady state position is much faster than that of the peak height (Fig.6(b) and (c)). Although this tendency has been found in the narrow slit case (Fig.4), it is much more enhanced in the wider slit case as seen in Fig.6. Figure 7 shows the steady state concentration profiles for $Pe = 0, 0.1, 0.3, 0.5, 1, 2$, and 3×10^{-3} in the polymer solution of $\bar{\phi}_p = 0.1$, $N = 1000$, $\chi = 0.5$, and slit width $L/R_g = 10$. These are numerical results obtained by the dynamic SCFT scheme described in Eq.(8) and

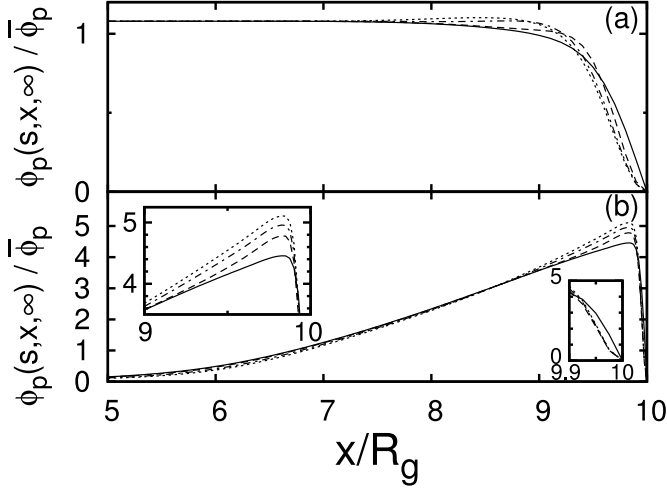


Fig. 8. Concentration profiles of s -th segment in the polymer solution ($\bar{\phi}_p = 0.1, N = 1000$ and $\chi = 0.5$) at steady states under (a) $Pe=0$ (no flow) and (b) $Pe=0.003$ in the region $5 \leq x/R_g \leq 10$. The lines are for $s = 0$ (solid line), 0.05 (dashed), 0.2 (dash dotted) and 0.5 (dotted). The two insets in (b) are the magnified figures of profiles near the downstream-side wall.

Eqs.(12)-(19). In addition, the peak concentration value and its position at steady state are shown as functions of Pe . For $Pe \gtrsim 1 \times 10^{-3}$ the peak position does not change much, but the peak height continues to increase with Pe , which indicates that the width of the segment accumulation becomes narrower while keeping the peak position almost the same as Pe increases, showing a strong depletion effect from the wall.

The individual segment concentration provides further details of the convective effect. From the statistical weight $q(x, s)$ obtained by Eq.(15) through the procedures (i)-(iv) we can calculate the concentration profile $\phi_p(s, x, t)$ for the s -th segment from

$$\phi_p(s, x, t) = \frac{V \bar{\phi}_p}{Q_p} q(s, x) q(1 - s, x). \quad (34)$$

Figure 8 shows the concentration profiles for the s -th segment at steady state of $s = 0.0$ (end point), 0.05 , 0.20 , and 0.5 (midpoint) under two conditions: (a) $Pe=0$ (no flow) and (b) $Pe=0.003$. Only the region $5 \leq x/R_g \leq 10$ is displayed. The profile for $Pe=0$ is symmetric about $x/R_g=5$, and for $Pe=0.003$ the concentration is quite small for $0 \leq x/R_g \leq 5$. The difference of the distributions among polymer segment concentrations is significantly enhanced by the flow. Furthermore, in the case of $Pe=0.003$, the distribution of the end segment ($s = 0$) is the broadest among others and the distributions for $0.1 \lesssim s < 0.5$ is similar to the case of $s = 0.5$ (midpoint) [2,35,36].

3.2 Good-solvent cases

For good-solvent condition ($v > 0$) under steady flow, the concentration profile can be obtained from Eq.(22) with

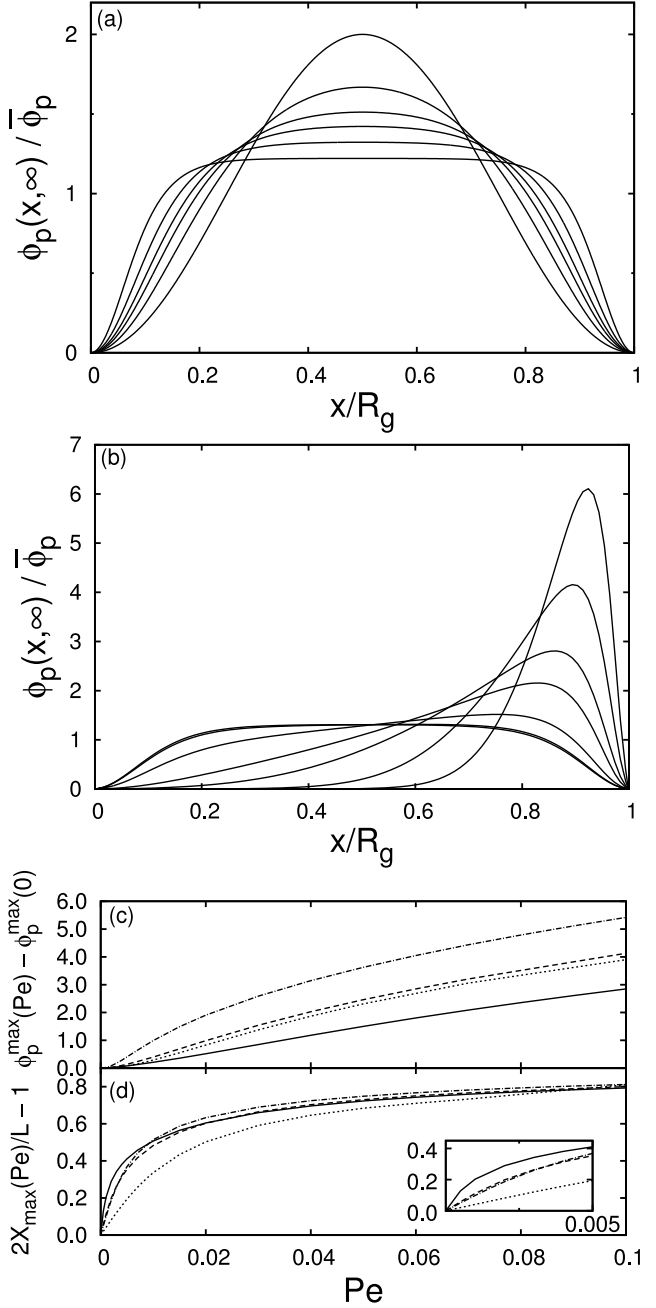


Fig. 9. Results for good solvent conditions. (a) Equilibrium ($Pe=0$) concentration profiles of polymer segments in good solvents with $\chi = -0.5, 0.0, 0.2, 0.3, 0.4$, and in Θ -solvent ($\chi = 0.5$) from the bottom to the top lines near the middle point. (b, c, d) Steady state behaviors of polymer solutions ($\bar{\phi}_p = 0.1, N = 1000$) in a narrow slit with $L/R_g = 1$ under steady flows with various Pe . The polymer segment volume fraction profiles (b) in $\chi = 0$ are for $Pe=0.0, 0.001, 0.01, 0.03, 0.05, 0.1, 0.2$, from left to right. The peak height (c) and the peak position (d) for $\chi=0$ (solid line), 0.3 (dashed line), are compared with the Θ -solvent ($\chi = 0.5, m = 1$) results, shown by the dotted line. As a reference, the case of $\chi = 0.5$, but with $m = 3/4$ is shown by the dash-dotted line.

$m = 3/4$. When $Pe=0$, we obtain the analytical concentration profile as (see Fig.9(a), details are given in Appendix A)

$$\phi_p(x) = [\varphi_m \text{sn}(\tilde{x}, k)]^2, \quad (35)$$

where φ_m is the maximum value of $\sqrt{\phi_p(x)}$, $\text{sn}(x, k)$ is the Jacobi elliptic integral, and $\tilde{x} = x\varphi_m\sqrt{v/2k^2}$. The constant k is defined by $k^2 = v\varphi_m^2/[2\mu_o(0) - v\varphi_m^2]$. Therefore from Eq.(26) we obtain the first-order asymptotic equation for the weak flow condition ($Pe \ll 1$):

$$\left[\frac{d^2}{d\tilde{x}^2} + k^2 + 1 - 6k^2 \text{sn}^2(\tilde{x}, k) \right] \tilde{\varphi}_1(\tilde{x}) = -\frac{L^2}{4K^2(k)} \text{sn}(\tilde{x}, k) \left[\mu_1(0) + \frac{1}{\sqrt{\phi_p}} \int_0^{\tilde{x}} \text{sn}(x', k) dx' \right] \quad (36)$$

where $\tilde{\varphi}_1 = \varphi_1/\varphi_m$. The constant $\mu_1(0)$ is determined by the normalization condition $\int_0^L \varphi^2(x) dx = L$. Unlike the Θ -solvent case, analytic approximations are extremely involved in this case, and thus concentration profiles in good solvents are obtained numerically for both weak and strong flow conditions. We again consider both narrow- and wide-slit cases next.

3.2.1 Narrow slit, $L/R_g = 1$

In Fig.9(b), we plot steady state volume fraction profiles $\phi_p(x)$ of a polymer solution in a narrow slit with $L/R_g = 1$ under various Pe . In Fig.9(c) and (d), both the peak height and position are plotted as functions of Pe for various χ -values. As a reference the Θ -solvent ($\chi = 0.5$, $m = 1$) result given in Fig.5 is shown by the dotted lines. In addition, the case of $\chi = 0.5$, but $m = 3/4$ is shown by the dash-dotted line for a comparison. From the comparison among the cases of $\chi = 0$, 0.3, and 0.5 with $m=3/4$ in Fig.9(c), we can see that the peak height of polymers concentration in a good solvent become less-sensitive to the convective effect with decreasing χ . This is because of the excluded volume effect in the good solvents. On the other hand, the behaviors of the peak height and position in the Θ -solvent are different from those in good-solvent conditions. The different behavior between the good- and Θ -solvents comes from the ϕ_p -dependent diffusion coefficient in Eq.(21). Namely, the flow in good solvents has a larger effective Peclet number by the factor $1/(\bar{\phi}_p)^{1/2}$ as seen from Eq.(21).

3.2.2 Wide slit, $L/R_g = 10$

Figure 10 shows the results for the same polymer solution in a wide slit with $L/R_g = 10$ and $0 \leq Pe \leq 0.01$. The peak concentration and position are plotted in Figures (b) and (c). As seen from (c), the profile is almost flat in the quiescent state and by applying a flow the peak position jumps from the center of the slit to a downstream position near the wall. The polymer segment profile is strongly influenced by the applied flow. Because the depletion width

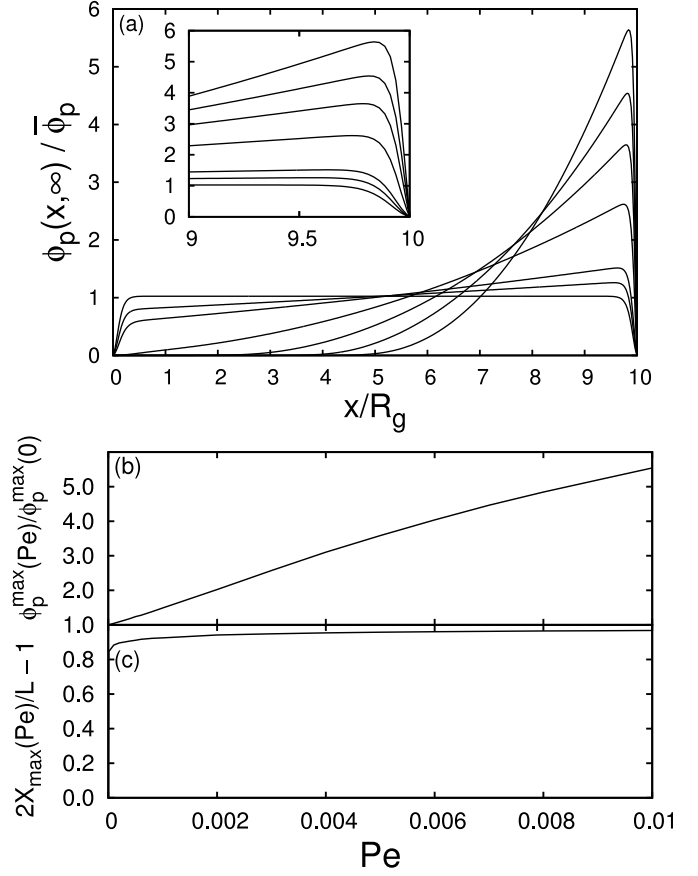


Fig. 10. (a) Steady state profiles of a polymer solution ($\bar{\phi}_p = 0.1$, $N = 1000$ and $\chi = 0$) in a wide slit with $L/R_g = 10$ under steady flows with $Pe=0, 0.5, 1, 3, 5, 7$, and 10×10^{-3} , from left to right, (b) the peak height $\phi_p^{max}(Pe)$ and (c) the peak position $x_{max}(Pe)$ of $\phi_p(x, \infty)$ as functions of Pe . The inset shows the result in the vicinity of the wall.

under good solvent conditions is relatively small compared with the slit width, the profile near the peak is very sharp. This is because the depletion thickness is reduced for good solvency by the larger excluded volume effect among the polymer chains.

4 Conclusions

A theoretical framework is presented based on a combination of the two-fluid model and self-consistent field theory to describe the polymer segment dynamics as a function of a flow field. We investigate a flow-induced concentration gradient in one direction only to illustrate the concept and demonstrate how the applied flow influences the polymer segment concentration profile under Θ - and good solvent conditions.

In the case of narrow slits, the ground state approximation is valid for Θ - and good solvent conditions. Under Θ -solvent conditions, we obtain analytic expression for the steady state volume fraction profile, valid up to the first

order in Peclet number Pe . For $Pe > 0.003$ flow significantly affects the polymer segment concentration profile between two walls. For the strong flow cases, we find that the peak position with respect to the steady state position shifts faster than the peak height of the concentration. In contrast to the peak height of the polymer concentration, the shift of the peak position in the range of small Pe ($\lesssim 0.005$) is well described by the first-order analytic approximation. Above $Pe \simeq 0.005$, the shift of peak position to the downstream side is suppressed. Under good solvent conditions, the concentration profile is now much more influenced compared to the Θ -solvent case. The depletion effect in a Θ -solvent is more significant compared to the good solvent case. This is because the depletion thickness in a good solvent condition is smaller due to the excluded volume effect between the polymer segments when the polymer concentration goes beyond the dilute regime.

For wide slit cases, the ground state approximation is no longer applicable to the Θ -solvent condition. We use the numerical dynamic self-consistent field theory in order to resolve the dynamics for such cases. With time the peak position compared to the steady state position shifts faster than concentration peak does. The concentration profile of segments that differ in ranking number along the chains shows that the difference among the polymer segment concentration distribution becomes larger when applying a flow field. For a flow with $Pe=0.003$, the distribution of the end segment is the broadest as compared to all other segments that tend to follow the distribution of the center-of-mass segments. For good solvency GSA is applicable, and the profile is strongly affected by flow. The peak position then gets very close to the wall on the downstream side. The model reveals transient relaxation and steady state features of the convective depletion dynamics. It will be of interest to validate these findings experimentally in the future.

Acknowledgment

This work was supported in part by KAKENHI from the Ministry of Education, Culture, Sports, Science and Technology of Japan, and by the U.S. NSF under Grant No. CMMI-0952646.

A Equilibrium profile in good solvents

The equilibrium profiles of polymer chains in a good solvent are described by Eq.(25). Multiplying Eq.(25) by $d\varphi_o/dx$ and then integrate it once, gives

$$\frac{1}{2} \left(\frac{d\varphi_o}{dx} \right)^2 + \frac{1}{2} \mu_o(0) \varphi_o^2 - \frac{1}{4} v \varphi_o^4 = C, \quad (37)$$

where C is a constant determined by $d\varphi_o/dx|_{x=L/2} = 0$ and $\varphi_o(L/2) = \varphi_m$ at the middle point. Hence $C = \varphi_m^2 \mu_p(0)/2 - \varphi_m^4 v/4$. Therefore, Eq.(37) becomes

$$\left(\frac{d\tilde{\varphi}_o}{d\tilde{x}} \right)^2 = (1 - \tilde{\varphi}_o^2)(1 - k^2 \tilde{\varphi}_o^2), \quad (38)$$

where $\tilde{\varphi}_o \equiv \varphi_o/\varphi_m$, $\tilde{x} = x\varphi_m\sqrt{v/2k^2}$, and k^2 is defined by

$$k^2 = \frac{v}{2\mu_o(0)/\varphi_m^2 - v}. \quad (39)$$

Integrating Eq.(38) yields

$$\tilde{\varphi}_o(\tilde{x}) = \text{sn}(\tilde{x}, k), \quad (40)$$

where $\text{sn}(x, k)$ is the Jacobi elliptic integral. From $\tilde{\varphi}_o = 1$ at $\tilde{x} = \tilde{L}/2$ we find $\tilde{L} = 2K(k)$ where $K(k)$ is the complete elliptic integral defined as

$$K(k) = \int_0^1 \frac{dt}{\sqrt{(1-t^2)(1-k^2t^2)}}, \quad (41)$$

and φ_m is expressed as

$$\varphi_m = \frac{2K(k)}{L} \sqrt{\frac{2k^2}{v}}. \quad (42)$$

From the normalization condition $\int_0^{L/2} \phi_o(x) dx = L/2$, we have

$$\frac{8k^2 K(k)}{vL^2} \int_0^{K(k)} \text{sn}^2(\tilde{x}, k) d\tilde{x} = 1. \quad (43)$$

Based on the properties of elliptic integrals it follows

$$K(k)(K(k) - E(k)) = \frac{v}{8} L^2, \quad (44)$$

where $E(k)$ is the second kind complete elliptic integral, expressed as

$$E(k) = \int_0^{\pi/2} \sqrt{1 - k^2 \sin^2 \varphi} d\varphi. \quad (45)$$

From Eqs.(39) and (42) we obtain

$$\mu_o(0) = \frac{4K^2(k)}{L^2} (k^2 + 1). \quad (46)$$

In summary, for a given v and L we can determine k from Eq.(44), and then evaluate φ_m and $\mu_o(0)$ from (42) and (46), respectively. The equilibrium profiles are zeroth-order solutions.

References

1. G.J. Fleer, M.A. Cohen Stuart, J.M.H.M. Scheutjens, T. Cosgrove, and B. Vincent. *Polymers at Interfaces*. (Chapman and Hall, New York, 1993).
2. E. Eisenriegler, J. Chem. Phys. **79**, (1983) 1052.
3. A. Hanke, E. Eisenriegler, and S. Dietrich, Phys. Rev. E **59**, (1999) 6853.
4. G.J. Fleer and R. Tuinier, Adv. Colloid Interface Sci. **143**, (2008) 1.
5. P.G. De Gennes, *Scaling Concepts in Polymer Physics* (Cornell University Press, Ithaca, 1979).

6. G.J. Fleer, A.M. Skvortsov, and R. Tuinier, *Macromolecules* **36**, (2003) 7857.
7. G.J. Fleer, A.M. Skvortsov, and R. Tuinier, *Macromol. Theory Sim.* **16**, (2007) 531 .
8. S. Asakura and F. Oosawa, *J. Chem. Phys.* **22**, (1954) 1255.
9. A. Vrij, *Pure Appl. Chem.* **48**, (1976) 471.
10. R. Verma, J.C. Crocker, T.C. Lubensky, and A.G. Yodh, *Macromolecules* **33**, (2000) 177.
11. H.N.W. Lekkerkerker, W.C.K. Poon, P.N. Pusey, A. Stroobants, and P. B. Warren, *Europhys. Lett.* **20**, (1992) 559.
12. S. M. Ilett, A. Orrock, W. C. K. Poon, and P. N. Pusey, *Phys. Rev. E* **51**, (1995) 1344 .
13. E. J. Meijer and D. Frenkel, *J. Chem. Phys.* **100**, (1994) 6873.
14. R. Tuinier, P.A. Smith, W.C.K. Poon, S.U. Egelhaaf, D.G.A.L. Aarts, H.N.W. Lekkerkerker, and G.J. Fleer, *Europhys. Lett.* **82**, (2008) 68002.
15. R. Tuinier and T. Taniguchi, *J. Phys: Condens. Matter* **L9**, (2005) 17.
16. U.S. Agarwal, A. Dutta, and R.A. Mashelkar, *Chem. Engin. Sci.* **49**, (1994) 1693.
17. H.A. Barnes, *J. Non-Newtonian Fluid Mech.* **56**, (1995) 221.
18. W.B. Gogarty, *J. Pet. Technol.* **35**, (1983) 1581; *ibid* **35**, (1983) 1767.
19. G. Chauveteau, *J. Rheol.* **26**, (1982) 111.
20. A. Omari, M. Moan, and G. Chauveteau, *Rheol. Acta* **28**, (1989) 520.
21. C.W. Macosko, *Rheology: Principles, Measurements and Applications*, (VCH Publishers, Inc., 1994).
22. M. Mooney, *Trans. Soc. Rheol.* **2**, (1931) 210.
23. R. Cheng, Y. Yang, and X. Yan, *Polymer* **40**, (1999) 3773.
24. E. Duerling and Y. Rabin, *Macromolecules* **23**, (1990) 2232.
25. R. Tuinier, J. K. G. Dhont, and T.-H. Fan, *Europhys. Lett.* **75**, (2006) 929.
26. T.-H. Fan, J. K. G. Dhont, and R. Tuinier, *Phys. Rev. E* **75**, (2007) 011803.
27. T.-H. Fan, R. Tuinier, *Soft Matter* **6**, (2010) 647.
28. T. Odijk, *Physica A* **337**, 389 (2004).
29. M. Doi and S.F. Edwards, *The Theory of Polymer Dynamics*. (Clarendon Press, Oxford 1986).
30. M. Doi and A. Onuki, *J. Phys. II France* **2**, (1992) 1631.
31. D. M. Hall, T. Lookman, G. H. Fredrickson and S. Banerjee, **244**, (2007) 681.
32. T. Taniguchi, T. Kawakatsu and K. Kawasaki, *AIP conference proceedings* **256**, (1992) 503.
33. E. Eisenriegler, A. Hanke and S. Dietrich, *J. Chem. Phys.*, **54**, 1134 (1996).
34. H. N. W. Lekkerkerker and R. Tuinier, *Colloids and the Depletion Interaction*, (Springer, Heidelberg 2011).
35. E. Eisenriegler, *Polymers near Surfaces*, (World Scientific, Singapore 1993).
36. E. Eisenriegler, *J. Chem. Phys.*, **116** 449 (2002).